

A THEORETICAL ANALYSIS FOR STATIC AND DYNAMIC BEHAVIOR OF FUNCTIONALLY GRADED PLATES

Tahar Hassaine Daouadji^{1,2*}, Abdeouahed Tounsi², Lazreg Hadji^{1,2},
Abdelaziz Hadj Henni^{1,2}, Adda Bedia El Abbès²

¹Université Ibn Khaldoun, BP 78 Zaaroura, 14000 Tiaret, Algérie.

²Laboratoire des Matériaux & Hydrologie, Université de Sidi Bel Abbès,
BP 89 Cité Ben M'hidi 22000 Sidi Bel Abbès, Algérie.

*e-mail: daouadjitah@yahoo.fr

Abstract. Theoretical formulation, Navier's solutions of rectangular plates based on a new higher order shear deformation model are presented for the static and dynamic analysis of functionally graded plates (FGPs). This theory enforces traction free boundary conditions at plate surfaces. Shear correction factors are not required because a correct representation of transverse shearing strain is given. Unlike any other theory, the number of unknown functions involved is only four, as against five in case of other shear deformation theories. The mechanical properties of the plate are assumed to vary continuously in the thickness direction by a simple power-law distribution in terms of the volume fractions of the constituents. Numerical illustrations concern flexural behavior of FG plates with Metal–Ceramic composition. Parametric studies are performed for varying ceramic volume fraction, volume fraction profiles, aspect ratios and length to thickness ratios. Results are verified with available results in the literature. It can be concluded that the proposed theory is accurate and simple in solving the static and dynamic behavior of functionally graded plates.

1. Introduction

The concept of functionally graded materials (FGMs) were the first introduced in 1984 by a group of material scientists in Japan, as ultrahigh temperature resistant materials for aircraft, space vehicles and other engineering applications. Functionally graded materials (FGMs) are new composite materials in which the micro-structural details are spatially varied through non-uniform distribution of the reinforcement phase. This is achieved by using reinforcement with different properties, sizes and shapes, as well as by interchanging the role of reinforcement and matrix phase in a continuous manner. The result is a microstructure that produces continuous or smooth change on thermal and mechanical properties at the macroscopic or continuum level (Koizumi [1]; Hirai and Chen [2]). Now, FGMs are developed for general use as structural components in extremely high temperature environments. Therefore, it is important to study the wave propagation of functionally graded materials structures in terms of non-destructive evaluation and material characterization.

Several studies have been performed to analyze the mechanical or the thermal or the thermo-mechanical responses of FG plates and shells. A comprehensive review is done by Tanigawa [3]. Reddy [4] has analyzed the static behavior of functionally graded rectangular plates based on his third-order shear deformation plate theory. Cheng and Batra [5] have related the deflections of a simply supported FG polygonal plate given by the first-order shear

2.1. Displacement fields and strains. The assumed displacement field is as follows:

$$\begin{aligned} u(x, y, z) &= u_0(x, y) - z \frac{\partial w_b}{\partial x} - f(z) \frac{\partial w_s}{\partial x}, \\ v(x, y, z) &= v_0(x, y) - z \frac{\partial w_b}{\partial y} - f(z) \frac{\partial w_s}{\partial y}, \end{aligned} \quad (1)$$

$$w(x, y, z) = w_b(x, y) + w_s(x, y),$$

where u_0 and v_0 are the mid-plane displacements of the plate in the x and y direction, respectively; w_b and w_s are the bending and shear components of transverse displacement, respectively, while $f(z)$ represents shape functions determining the distribution of the transverse shear strains and stresses along the thickness and is given as:

$$f(z) = z \left[1 + \frac{3\pi}{2} \sec^2 h^2 \left(\frac{1}{2} \right) \right] - \frac{3\pi}{2} h \tanh \left(\frac{z}{h} \right). \quad (2)$$

It should be noted that unlike the first-order shear deformation theory, this theory does not require shear correction factors. The kinematic relations can be obtained as follows:

$$\begin{aligned} \varepsilon_x &= \varepsilon_x^0 + z k_x^b + f(z) k_x^s, \\ \varepsilon_y &= \varepsilon_y^0 + z k_y^b + f(z) k_y^s, \\ \gamma_{xy} &= \gamma_{xy}^0 + z k_{xy}^b + f(z) k_{xy}^s, \\ \gamma_{yz} &= g(z) \gamma_{yz}^s, \\ \gamma_{xz} &= g(z) \gamma_{xz}^s, \\ \varepsilon_z &= 0, \end{aligned} \quad (3)$$

where

$$\begin{aligned} \varepsilon_x^0 &= \frac{\partial u_0}{\partial x}, \quad k_x^b = -\frac{\partial^2 w_b}{\partial x^2}, \quad k_x^s = -\frac{\partial^2 w_s}{\partial x^2}, \\ \varepsilon_y^0 &= \frac{\partial v_0}{\partial y}, \quad k_y^b = -\frac{\partial^2 w_b}{\partial y^2}, \quad k_y^s = -\frac{\partial^2 w_s}{\partial y^2}, \\ \gamma_{xy}^0 &= \frac{\partial u_0}{\partial y} + \frac{\partial v_0}{\partial x}, \quad k_{xy}^b = -2 \frac{\partial^2 w_b}{\partial x \partial y}, \quad k_{xy}^s = -2 \frac{\partial^2 w_s}{\partial x \partial y}, \end{aligned} \quad (4)$$

$$\begin{Bmatrix} N_x \\ M_x^b \\ M_x^s \end{Bmatrix}, \begin{Bmatrix} N_y \\ M_y^b \\ M_y^s \end{Bmatrix}, \begin{Bmatrix} N_{xy} \\ M_{xy}^b \\ M_{xy}^s \end{Bmatrix} = \int_{-h/2}^{h/2} (\sigma_x, \sigma_y, \tau_{xy}) \begin{Bmatrix} 1 \\ z \\ f(z) \end{Bmatrix} dz, \quad (10a)$$

$$(S_{xz}^s, S_{yz}^s) = \int_{-h/2}^{h/2} (\tau_{xz}, \tau_{yz}) g(z) dz. \quad (10b)$$

The governing equations of equilibrium can be derived from Eq. (9) by integrating the displacement gradients by parts and setting the coefficients δu_0 , δv_0 , δw_b , and δw_s zero separately. Thus one can obtain the equilibrium equations associated with the present shear deformation theory,

$$\begin{aligned} \delta u: \quad & \frac{\partial N_x}{\partial x} + \frac{\partial N_{xy}}{\partial y} = 0, \\ \delta v: \quad & \frac{\partial N_{xy}}{\partial x} + \frac{\partial N_y}{\partial y} = 0, \\ \delta w_b: \quad & \frac{\partial^2 M_x^b}{\partial x^2} + 2 \frac{\partial^2 M_{xy}^b}{\partial x \partial y} + \frac{\partial^2 M_y^b}{\partial y^2} + q = 0, \\ \delta w_s: \quad & \frac{\partial^2 M_x^s}{\partial x^2} + 2 \frac{\partial^2 M_{xy}^s}{\partial x \partial y} + \frac{\partial^2 M_y^s}{\partial y^2} + \frac{\partial S_{xz}^s}{\partial x} + \frac{\partial S_{yz}^s}{\partial y} + q = 0. \end{aligned} \quad (11)$$

Using Eq. (6) in Eq. (10), the stress resultants of a sandwich plate made up of three layers can be related to the total strains by

$$\begin{Bmatrix} N \\ M^b \\ M^s \end{Bmatrix} = \begin{bmatrix} A & B & B^s \\ A & D & D^s \\ B^s & D^s & H^s \end{bmatrix} \begin{Bmatrix} \varepsilon \\ k^b \\ k^s \end{Bmatrix}, \quad S = A^s \gamma, \quad (12)$$

where

$$N = \{N_x, N_y, N_{xy}\}^t, \quad M^b = \{M_x^b, M_y^b, M_{xy}^b\}^t, \quad M^s = \{M_x^s, M_y^s, M_{xy}^s\}^t, \quad (13a)$$

$$\varepsilon = \{\varepsilon_x^0, \varepsilon_y^0, \gamma_{xy}^0\}^t, \quad k^b = \{k_x^b, k_y^b, k_{xy}^b\}^t, \quad k^s = \{k_x^s, k_y^s, k_{xy}^s\}^t, \quad (13b)$$

$$A = \begin{bmatrix} A_{11} & A_{12} & 0 \\ A_{12} & A_{22} & 0 \\ 0 & 0 & A_{66} \end{bmatrix}, \quad B = \begin{bmatrix} B_{11} & B_{12} & 0 \\ B_{12} & B_{22} & 0 \\ 0 & 0 & B_{66} \end{bmatrix}, \quad D = \begin{bmatrix} D_{11} & D_{12} & 0 \\ D_{12} & D_{22} & 0 \\ 0 & 0 & D_{66} \end{bmatrix}, \quad (13c)$$

2.4. Exact solution for a simply-supported FGM plate. Rectangular plates are generally classified in accordance with the type of support used. We are here concerned with the exact solution of Eqs. (15a–d) for a simply supported FG plate. The following boundary conditions are imposed at the side edges:

$$v_0 = w_b = w_s = \frac{\partial w_s}{\partial y} = N_x = M_x^b = M_x^s = 0 \quad \text{at } x = -a/2, a/2, \quad (17a)$$

$$u_0 = w_b = w_s = \frac{\partial w_s}{\partial x} = N_y = M_y^b = M_y^s = 0 \quad \text{at } y = -b/2, b/2. \quad (17b)$$

To solve this problem, Navier assumed that the transverse mechanical and temperature loads, q in the form of a double trigonometric series as

$$q = q_0 \sin(\lambda x) \sin(\mu y), \quad (18)$$

where $\lambda = m\pi/a$, $\mu = n\pi/b$, and q_0 represents the intensity of the load at the plate center.

Following the Navier solution procedure, we assume the following solution form for u_0 , v_0 , w_b and w_s that satisfies the boundary conditions,

$$\begin{Bmatrix} u_0 \\ v_0 \\ w_b \\ w_s \end{Bmatrix} = \begin{Bmatrix} U \cos(\lambda x) \sin(\mu y).e^{i\omega t} \\ V \sin(\lambda x) \cos(\mu y).e^{i\omega t} \\ W_b \sin(\lambda x) \sin(\mu y).e^{i\omega t} \\ W_s \sin(\lambda x) \sin(\mu y).e^{i\omega t} \end{Bmatrix}, \quad (19)$$

where ω is the natural frequency and U , V , W_b , and W_s are arbitrary parameters to be determined subjected to the condition that the solution in Eq. (19) satisfies governing Eqs. (15). Equation (19) reduces the governing equations to the following form:

For flexural analysis,

$$[C]\{\Delta\} = \{P\}, \quad (20a)$$

And for vibration analysis,

$$([C] - \omega[G])\{\Delta\} = \{0\}, \quad (20b)$$

where $\{\Delta\} = \{U, V, W_b, W_s\}^t$, $[C]$ and $[G]$ refers to the flexural stiffness and mass matrices and ω to the corresponding frequency.

$$[C] = \begin{bmatrix} a_{11} & a_{12} & a_{13} & a_{14} \\ a_{12} & a_{22} & a_{23} & a_{24} \\ a_{13} & a_{23} & a_{33} & a_{34} \\ a_{14} & a_{24} & a_{34} & a_{44} \end{bmatrix}, \quad [G] = \begin{bmatrix} m_{11} & 0 & 0 & 0 \\ 0 & m_{22} & 0 & 0 \\ 0 & 0 & m_{33} & m_{34} \\ 0 & 0 & m_{34} & m_{44} \end{bmatrix}, \quad (21)$$

$$q = q_0 \sin\left(\frac{m\pi}{a} x\right) \sin\left(\frac{n\pi}{b} y\right), \quad (24)$$

where q_0 represents the intensity of the load at the plate center.

A functionally graded material consisting of Aluminum - Alumina is considered. The following material properties are used in computing the numerical values (Bouazza et al. [12]): Metal (Aluminium, Al): $E_m = 70$ GPa; Poisson's ratio $\nu = 0.3$;

Ceramic (Alumina, Al_2O_3): $E_c = 380$ GPa; Poisson's ratio $\nu = 0.3$.

Now, a functionally graded material consisting of aluminum and alumina is considered. Young's modulus for aluminum is 70 GPa while for alumina is 380 GPa. Note that, Poisson's ratio is selected constant for both and equal to 0.3. The various non-dimensional parameters used are

$$\begin{aligned} \bar{w} &= \frac{10 h^3 Ec}{a^4 q_0} w\left(\frac{a}{2}, \frac{b}{2}\right), & \bar{u}_x &= \frac{100 h^3 Ec}{a^4 q_0} u_x\left(\frac{a}{2}, \frac{b}{2}, -\frac{h}{4}\right), \\ \bar{u}_y &= \frac{100 h^3 Ec}{a^4 q_0} u_y\left(\frac{a}{2}, \frac{b}{2}, -\frac{h}{6}\right), & \bar{\sigma}_x &= \frac{h}{aq_0} \sigma_x\left(\frac{a}{2}, \frac{b}{2}, \frac{h}{2}\right), \\ \bar{\sigma}_y &= \frac{h}{aq_0} \sigma_y\left(\frac{a}{2}, \frac{b}{2}, \frac{h}{3}\right), & \bar{\tau}_{xy} &= \frac{h}{aq_0} \tau_{xy}\left(0, 0, -\frac{h}{3}\right), \\ \bar{\tau}_{yz} &= \frac{h}{aq_0} \tau_{yz}\left(\frac{a}{2}, 0, \frac{h}{6}\right), & \bar{\tau}_{xz} &= \frac{h}{aq_0} \tau_{xz}\left(0, \frac{b}{2}, 0\right). \end{aligned} \quad (25)$$

It is clear that the deflection increases as the side-to-thickness ratio decreases. The same results were obtained in most literatures. In addition, the correlation between the present new higher order shear deformation theory and different higher-order and first-order shear deformation theories is established by the author in his recent papers. It is found that this theory predicts the deflections and stresses more accurately when compared to the first and third-order theories.

For the sake of completeness, results of the present theory are compared with those obtained using a new Navier-type three-dimensionally exact solution for small deflections in bending of linear elastic isotropic homogeneous rectangular plates. The center deflection w and the distribution across the plate thickness of in-plane longitudinal stress σ_x and longitudinal tangential stress τ_{xy} are compared with the results of the 3-D [13] solution and are shown in Table 1 and Table 2. The present solution is realized for a quadratic plate, with the following fixed data: $a = 1$, $b = 1$, $E_m = E_c = E = 1$, $q_0 = 1$, $\nu = 0.3$ and three values for the plate thickness: $h = 0.01$, $h = 0.03$ and $h = 0.1$. It is to be noted that the present results compare very well with the 3-D solution [13]. All deflections again compare well with the 3-D solution, and show good convergence with the average 3-D solution.

Table 1. Center deflections of isotropic homogenous plates ($k=0$, $E_m=E_c=E=1$ and $a/b=1$).

h/a	CPT [14]	3D [13], $z=0$	SSDPT [6]	Present theory NHPSDT	Reddy [4]
0.01	44360.9	44384.7	44383.84	44383.86	44383.87
0.03	1643.00	1650.94	1650.646	1650.652	1650.657
0.1	44.3609	46.7443	46.6548	46.65655	46.65836

Table 3. Effects of volume fraction exponent and loading on the dimensionless stresses and displacements of a FGM square plate ($a/h=10$).

k	Theory	w	σ_x	σ_y	τ_{yz}	τ_{xz}	τ_{xy}
0 ceramic	NHPSDT(present)	0.4665	2.8928	1.9104	0.4424	0.5072	1.2851
	SSDPT [6]	0.4665	2.8932	1.9103	0.4429	0.5114	1.2850
	Reddy [4]	0.4665	2.8920	1.9106	0.4411	0.4963	1.2855
1	NHPSDT(present)	0.9421	4.2607	2.2569	0.54404	0.50721	1.1573
	SSDPT [6]	0.9287	4.4745	2.1692	0.5446	0.5114	1.1143
	Reddy [4]	0.94214	4.25982	2.25693	0.54246	0.49630	1.15725
2	NHPSDT(present)	1.2228	4.8890	2.1663	0.5719	0.4651	1.0448
	SSDPT [6]	1.1940	5.2296	2.0338	0.5734	0.4700	0.9907
	Reddy [4]	1.22275	4.88814	2.16630	0.56859	0.45384	1.04486
3	NHPSDT(present)	1.3533	5.2064	1.9922	0.56078	0.4316	1.0632
	SSDPT [6]	1.3200	5.6108	1.8593	0.5629	0.4367	1.0047
	Reddy [4]	1.3530	5.20552	1.99218	0.55573	0.41981	1.06319
5	NHPSDT(present)	1.4653	5.7074	1.7143	0.50075	0.4128	1.1016
	SSDPT [6]	1.4356	6.1504	1.6104	0.5031	0.4177	1.0451
	Reddy [4]	1.46467	5.70653	1.71444	0.49495	0.40039	1.10162
10	NHPSDT(present)	1.6057	6.9547	1.3346	0.4215	0.4512	1.1118
	SSDPT [6]	1.5876	7.3689	1.2820	0.4227	0.4552	1.0694
	Reddy [4]	1.60541	6.95396	1.33495	0.41802	0.43915	1.1119
∞ metal	NHPSDT(present)	2.5327	2.8928	1.9104	0.4424	0.5072	1.2851
	SSDPT [6]	2.5327	2.8932	1.9103	0.4429	0.5114	1.2850
	Reddy [4]	2.5328	2.8920	1.9106	0.4411	0.4963	1.2855

Table 4. Comparison of normalized displacements and stresses of a FGM square plate ($a/b=1$) and $k=0$.

a/h	Theory	w	σ_x	σ_y	τ_{yz}	τ_{xz}	τ_{xy}
4	NHPSDT(present)	0.5866	1.1979	0.7536	0.4307	0.4937	0.4908
	SSDPT [6]	0.5865	1.1988	0.7534	0.4307	0.4973	0.4906
	Reddy [4]	0.5868	1.1959	0.7541	0.4304	0.4842	0.4913
10	NHPSDT(present)	0.4665	2.8928	1.9104	0.4424	0.5072	1.2851
	SSDPT [6]	0.4665	2.8932	1.9103	0.4429	0.5114	1.2850
	Reddy [4]	0.4666	2.8920	1.9106	0.4411	0.4963	1.2855
100	NHPSDT(present)	0.4438	28.7342	19.1543	0.4466	0.5119	12.9884
	SSDPT [6]	0.4438	28.7342	19.1543	0.4472	0.5164	13.0125
	Reddy [4]	0.4438	28.7341	19.1543	0.4448	0.5004	12.9885

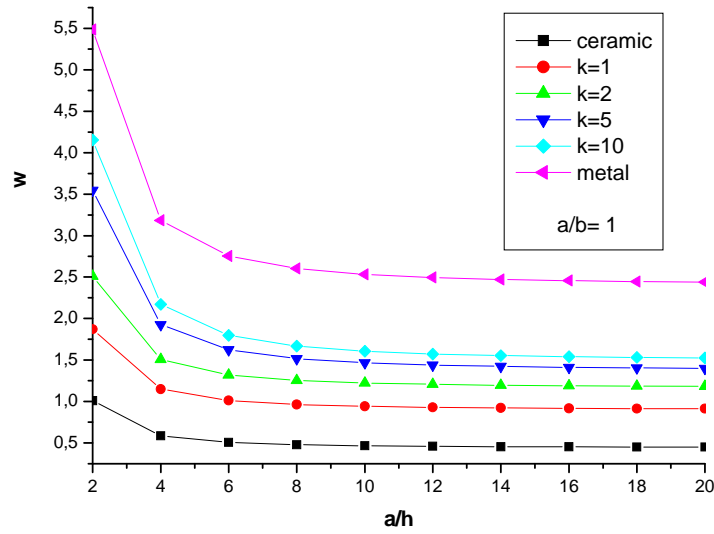


Fig. 3. Dimensionless center deflection (w) as a function of the side-to-thickness ratio (a/h) of FGM square plate.

Figures 4 and 5 depict the through-the-thickness distributions of the shear stresses τ_{yz} and τ_{xz} ; the in plane longitudinal and normal stresses σ_x and σ_y , and the longitudinal tangential stress τ_{xy} in the FGM plate under the uniform load. The volume fraction exponent of the FGM plate is taken as $k = 2$ in these figures. Distinction between the curves in Figs. 5 and 6 is obvious. As strain gradients increase, the in homogeneities play a greater role in stress distribution calculations. The through-the-thickness distributions of the shear stresses τ_{yz} and τ_{xz} are not parabolic and the stresses increase as the aspect ratio decreases. It is to be noted that the maximum value occurs at $z \cong 0.2$, not at the plate center as in the homogeneous case.

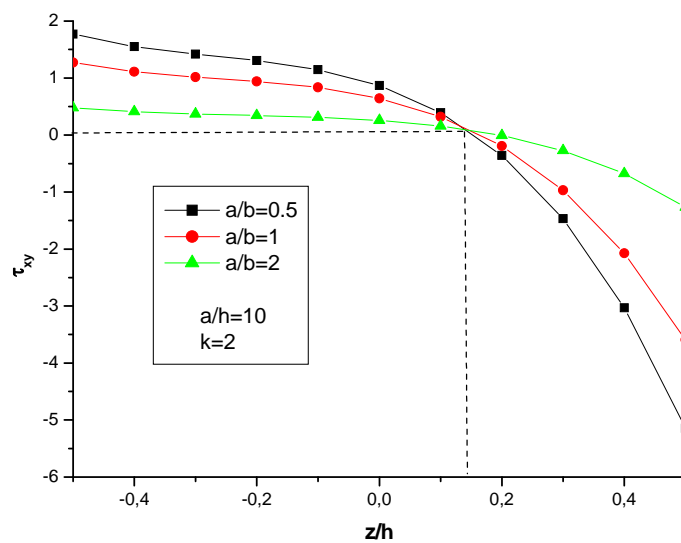


Fig. 4. Variation of longitudinal tangential stress (τ_{xy}) through the thickness of FGM plate for different values of the aspect ratio.

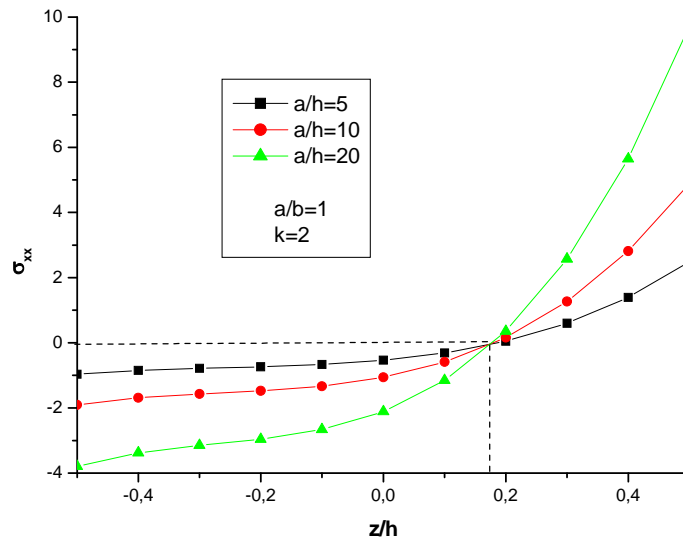


Fig. 7. Variation of in-plane longitudinal stress (σ_{xx}) through-the thickness of FGM plate for different values of the side -to-thickness ratio.

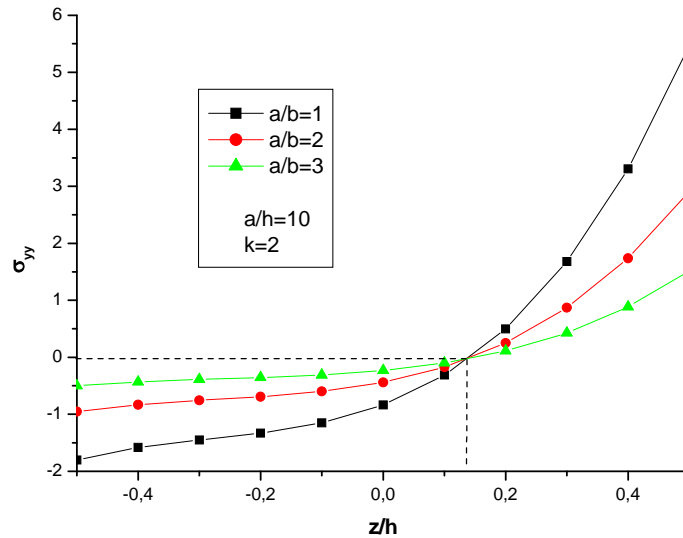


Fig. 8. Variation of in-plane normal stress (σ_{yy}) through-the thickness of FGM plate for different values of the aspect ratio.

Finally, the exact maximum deflections of simply supported FGM square plate are compared in Fig. 9 for various ratios of module, Em/Ec (for a given thickness, $a/h = 10$). This means that the deflections are computed for plates with different ceramic–metal mixtures. It is clear that the deflections decrease smoothly as the volume fraction exponent decreases and as the ratio of metal-to-ceramic modules increases.

Several parameters are varied and their dynamic behavior is studied. The first three natural frequencies for the fundamental vibration mode of $m=n=1$ of a square Al / Al₂O₃ FG plate are compared with the corresponding results of 3D analysis by Vel et al [17] in Table 6. The Table 6 also presents the results obtained by Matsunaga's theory [15] and Reddy's HSDT [4].

Table 7 presents the effect of power law index on dimensionless frequency. From these tables it is evident that the present theory predicts results more accurately than the other models when compared with 3D elasticity solutions.

Table 7. Effect of power law index on fundamental frequencies of Al/Al₂O₃ FG square plates^{*)}.

	Power law index n							
	$n = 1$		2		3		5	
NHPSDT(present)	5.6777		5.6229		5.6385		5.6651	
UNSDT [15]	5.882		5.8907		5.889		5.8523	
Reddy [4]	5.6914		5.6421		5.6571		5.6795	
HSDT [16]	5.7123		5.6599		5.6757		5.702	
3D [17]	5.4806		5.4923		5.5285		5.5632	
Source	$n = 1$	% error	2	% error	3	% error	5	% error
NHPSDT(present)	5.6777	3.59	5.6229	2.38	5.6385	1.99	5.6651	1.83
UNSDT [15]	5.882	7.32	5.8907	7.25	5.889	6.52	5.8523	5.20
Reddy [4]	5.6914	3.85	5.6421	2.73	5.6571	2.33	5.6795	2.09
HSDT [16]	5.7123	4.23	5.6599	3.05	5.6757	2.66	5.702	2.49
3D [17]	5.4806	0.00	5.4923	0.00	5.5285	0.00	5.5632	0.00

$$*) \bar{\omega} = \left(\omega \left(\frac{a^2}{h} \right) \sqrt{\frac{\rho_m}{E_m}} \right), a/h = 5.$$

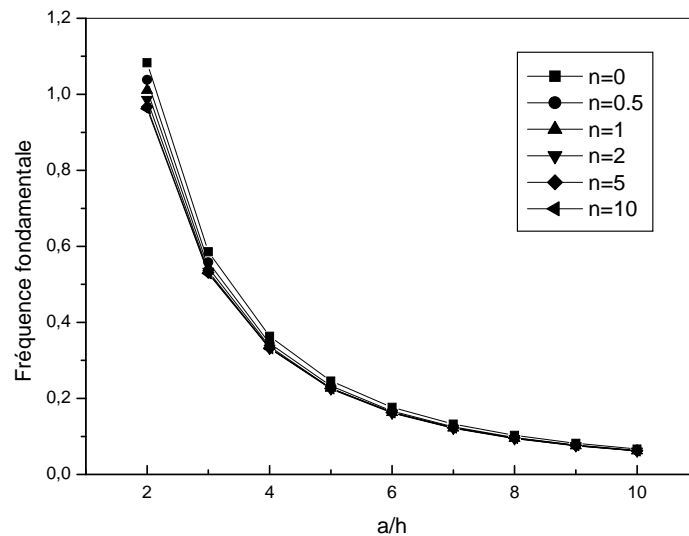


Fig. 10. Dimensionless Frequency $\left(\bar{\omega} = \omega h \sqrt{\frac{\rho_m}{E_m}} \right)$ as function of side to thickness ratio a/h for various power law index of FGM square plates.

Effect of side to thickness ratio (a/h), aspect ratio (a/b) and modulus ratio (E_m/E_c) on fundamental frequencies are show in Figs. 10, 11 and 12.

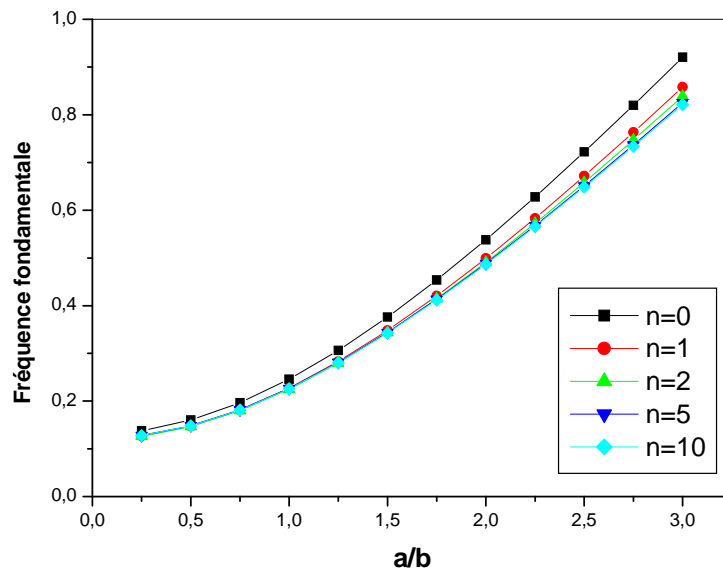


Fig. 11. Dimensionless Frequency $\left(\bar{\omega} = \omega h \sqrt{\frac{\rho_m}{E_m}}\right)$ as function of aspect ratio a/b for various power law index of FGM square plates $a/h = 5$.

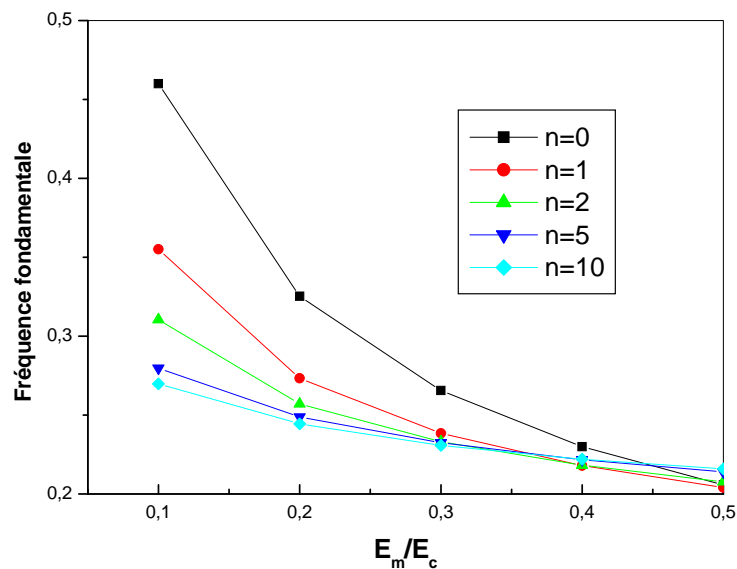


Fig. 12. Dimensionless Frequency $\left(\bar{\omega} = \omega h \sqrt{\frac{\rho_m}{E_m}}\right)$ as function of modulus ratio E_m/E_c for various power law index of FGM square plates $a/h = 5$.

5. Conclusion

This paper presents, a new higher order shear deformation model is proposed to analyze the static and dynamic behavior of functionally graded plates. Navier solutions for flexure and free vibration analysis of FG plates are presented. The stresses and displacements are computed for plates with Metal–Ceramic mixture and it is seen that the response is intermediate to that of metal and ceramic. Hence the gradients in material properties play a vital role in determining the response of FGM plates it may be concluded that the present model provides better estimates for the deflections and stresses than that of a generalized shear Deformation Theory [15] and very close to the solutions obtained with that of Reddy's higher order model [4].

All comparison studies demonstrated that the deflections and stresses obtained using the present new higher order shear deformation theories (with four unknowns) and other higher shear deformation theories (with five unknowns) are almost identical. This model is also used for predicting fundamental frequencies of FG plates. The influence played by plate aspect ratio, side to thickness ratio and modulus ratio are studied. The present model provides results in excellent agreement with the available results and gives a better estimates than the other accepted models [6-15] when compared with 3D elasticity solutions. The extension of the present theory is also envisaged for general boundary conditions and plates of a more general shape. In conclusion, it can be said that the proposed theory NHPSDT is accurate and simple in solving the static behaviors of FGM plates.

References

- [1] M. Koizumi // *Ceramic Transactions, Functionally Gradient Materials* **34** (1993) 3.
- [2] T. Hirai, L. Chen // *Materials Science Forum* **308-311**(1999) 509.
- [3] Y. Tanigawa // *Appl. Math. Mech.* **48** (1995) 287.
- [4] J.N. Reddy // *Internanional Journal of Numerical Methods in Engineering* **68** (2000) 643.
- [5] Z.Q. Cheng, R.C. Batra // *Arch. Mech.* **52** (2000) 143.
- [6] A.M. Zenkour // *Applied Mathematical Modelling* **30** (2006) 67.
- [7] M. Şimşek // *Compos. Struct.* **92** (2010) 904.
- [8] M. Şimşek // *Nuclear Engineering and Design* **240** (2010) 697.
- [9] A. Benachour, T. Hassaine Daouadji, H. Ait Atmane, A. Tounsi, S.A. Meftah // *Composites B: Engineering* **42** (2011) 1386.
- [10] H.H. Abdelaziz, H. Ait Atmane, I. Mechab, L. Boumia, A. Tounsi, E.A. Adda Bedia // *Chinese journal of aeronautics* **24** (2011) 434.
- [11] M. Şimşek // *Compos. Struct.* **92** (2010) 2532.
- [12] M. Bouazza, A. Tounsi, E.A. Adda Bedia, M. Meguenni // *Advanced Structures Materials B* **15** (2011) 669.
- [13] H. Werner // *Commun. Numer. Methods Eng.* **15** (1999) 295.
- [14] S.P. Timoshenko, S. Woinowsky-Krieger, *Theory of Plates and Shells* (McGraw-Hill, New York, 1959).
- [15] H. Matsunaga // *Composite Structures* **84** (2008) 132.
- [16] K.N. Trung, Karam Sab, Guy Bonnet // *Composite Structures* **83** (2008) 25.
- [17] S.S. Vel, R.C. Batra // *Journal of Sound and Vibration* **272(3)** (2004) 703.